JOURNAL OF SOLID STATE CHEMISTRY 25, 329–346 (1978)

Origin of the Quadrupole Splitting in the Mössbauer ^{57}Fe Spectrum of Cubic (Disordered) $LiFeO_2$

OSVALD KNOP,* CONRAD AYASSE,† J. S. CARLOW,‡ AND W. W. BARKER§

Department of Chemistry, Dalhousie University, Halifax, Nova Scotia, Canada B3H 4J3

F. W. D. WOODHAMS

Department of Natural Philosophy, Aberdeen University, Aberdeen, Scotland AB9 2UE

AND R. E. MEADS AND W. G. PARKER

Department of Physics, University of Exeter, Exeter, England EX4 4QL

Received November 4, 1977

The room-temperature Mössbauer ^{57}Fe spectrum of polycrystalline disordered cubic α-$LiFeO_2$ contains a quadrupole splitting $|\Delta_{obs}|$ of 0.65(2) mm/sec. This value is relatively large for an Fe atom in an essentially Fe^{3+}_{HS} state. To account for its magnitude, the distribution of the electric-field gradient (EFG) values associated with the Fe atoms was investigated by means of exact geometric analysis involving the 12 nearest cation neighbors (model A) as well as large-scale computer simulation involving more distant cations (models B to E). It is found that (1) the major contribution to $|\Delta_{obs}|$ comes from the distribution of +1 and +3 charges among the 12 nearest cation neighbors of a reference Fe atom; (2) this contribution by itself largely accounts for $|\Delta_{obs}|$; (3) the contribution from cations beyond the seventh-nearest neighbors is marginal; (4) displacing the oxygen atoms from their lattice sites toward adjacent Fe atoms produces a significant effect on the distribution of EFG values at a reference Fe atom, while incipient cation ordering appears to have a relatively small effect; and (5) the contribution of the EFG = 0 component to model |EFG| distributions will be overemphasized unless cations beyond the first-nearest neighbors are included in the EFG summation. The 144 distinct (up to rotation and reflection) $Li^{1+}_{12-k}Fe^{3+}_{k}$ configurations on the coordination cuboctahedron of nearest cation neighbors (required for the examination of model A) are listed, together with their symmetries and multiplicities, and it is shown that the 144 configurations engender only 17 distinct |EFG| values. Observations are also made on various geometric aspects of calculating EFG at $^{57}Fe^{3+}_{HS}$ on cubic lattices.

The general aim of this work is to explore the possibility of predicting, from simple and modified point-charge models, the magnitude of the quadrupole splitting due to random distribution of ionic charges in disordered solid solutions. Specifically, we attempt to account for the quadrupole splitting observed in the Mössbauer ^{57}Fe spectrum of the cubic phase of $LiFeO_2$.

Cubic (α) $LiFeO_2$ is a quenchable high-temperature phase with a structure of the NaCl type, $a \approx 4.16$ Å, and a statistical

* To whom correspondence may be addressed.

† Holder of a Killam Graduate Scholarship, 1969–1971.

‡ Killam Postdoctoral Fellow, 1972–1974. Present address: S. B. Division, CERN, 1211 Geneva 23, Switzerland.

§ Killam Postdoctoral Fellow, 1968–1970. Present address: Minerals Research Laboratories, Division of Mineralogy, CSIRO, Wembley, W.A. 6014, Australia.

0022-4596/78/0254/0329/$02.00/0

distribution of the Li^{1+} and Fe^{3+} ions over the cation sublattices. Its room-temperature Mössbauer ^{57}Fe spectrum was reported by Cox *et al.* (*1*) as consisting of a partially resolved doublet with a quadrupole splitting $|\Delta|$ of 0.56(5) mm/sec and an isomer shift δ characteristic of high-spin Fe^{3+}. The splitting remained constant between about 90 and 520°K. Cox *et al.* find the existence and magnitude of the splitting and the sharpness of the components of the doublet (estimated linewidths, 0.50 mm/sec) surprising. In their own words, "The S state of the Fe^{3+} ion makes the present effect [i.e., the existence of a quadrupole splitting in a pseudocubic environment] in $LiFeO_2$, particularly the well-defined value of Δ, rather difficult to understand. The origin of the effect very probably lies in the drastically asymmetric charge distribution associated with the random distribution of Li^{1+} and Fe^{3+} on neighboring equivalent sites, but Δ might then be expected to have different values according to the particular numbers and distribution of these ions surrounding a given Fe ion."

In the following we investigate to what extent the observed splitting *is* attributable to a distribution of environments of an Fe atom in the disordered structure. The splitting in the spectrum of a polycrystalline specimen depends on the electric-field gradient g at the ^{57}Fe nucleus:

$$\Delta(^{57}\mathrm{Fe}) = \tfrac{1}{2}e^2Qg, \qquad g = |q|(1 + \eta^2/3)^{1/2}, \quad (1)$$

$$q = (1 - R)q_{\mathrm{val}} + (1 - \gamma_\infty)q_{\mathrm{latt}}, \quad (2)$$

$$\eta q = (1 - R)\eta_{\mathrm{val}}q_{\mathrm{val}} + (1 - \gamma_\infty)\eta_{\mathrm{latt}}q_{\mathrm{latt}}. \quad (3)$$

For reasons outlined later, we concern outselves with the lattice terms to the exclusion of the valence terms, so that for our purpose $q \propto q_{\mathrm{latt}}$ and $\Delta \propto q_{\mathrm{latt}}$. The quantity $g_{\mathrm{latt}} = q_{\mathrm{latt}}(1 + \eta_{\mathrm{latt}}^2/3)^{1/2}$ (in $Å^{-3}$) is referred to as EFG; hence $|\Delta| \propto |\mathrm{EFG}|$. The crystal is assumed purely ionic, with the formal charges u (in units of e) on the Li, Fe, and O atoms of +1, +3, and −2, respectively, and the EFG values refer to $\frac{1}{2}a(\alpha\text{-}LiFeO_2) = 2.08$ Å throughout except where stated otherwise. The following models are examined:

(A) The unmodified point-charge model. All atoms are at the lattice sites of an idealized NaCl-type structure at 0°K, and the cations are distributed completely at random. No contribution to the EFG at an Fe nucleus is made by the O^{2-} ions. Only the effect of the first-nearest cation neighbors is considered, but it is based upon an exact geometric analysis.

(B) The examination of model A is extended to include the contribution to EFG of more distant cations. Since an exact geometric analysis involving even the second-nearest cation neighbors is not feasible (see below), direct computer simulation is employed using sufficiently large samples of the idealized $LiFeO_2$ structure. The simulation is carried out in two ways:

(1) A cubic block of the structure is generated, and Li and Fe atoms are placed at the cation sites at random. The EFG due to all the cations is computed at a cation site at the centre of the block. Repeating the process a number of times yields a distribution of EFG values which approximates the distribution in a sample of infinite extension.

(2) A large sample of the structure is generated, and the cation sites are populated at random by Li and Fe atoms. The cation environment of each atom (cyclic boundary conditions applied) is searched within a sphere of specified radius r_{max}, and the EFG due to the cations within the sphere is computed. In this manner one can investigate the convergence of the EFG distribution with r_{max}.

(C) Each oxygen ion in sample B2 is displaced from its lattice point by a specified amount toward its neighboring cation of higher charge, and the EFG at each Fe atom due to the cations *and* oxygens within a sphere of specified radius r_{max} is computed.

(D) A specified degree of cationic order is introduced into sample B2; otherwise as in B2.

(E) The oxygens in model D are displaced as in model C.

The isomer shift is assumed to be independent of the environment of an Fe atom in all the models.

The geometric analysis implicit in the treatment of model A is applicable to any situation which involves a coordination cuboctahedron of composition $X_{12-k}Y_k$, e.g., the coordination cuboctahedron around the A atom in random cubic perovskites $AB(X,Y)_3$, where the anions X and Y have different charges. It is similar to, but considerably more complicated than, the analysis which yields the familiar results for the coordination octahedron $X_{6-k}Y_k$ and is therefore described in some detail.

The effect of anion displacement and of partial cationic order on the distribution of EFG values in a disordered solid solution has not, to our knowledge, been investigated previously. Since this effect is of interest in its own right and its nature and magnitude are difficult to anticipate, we first ascertain and describe its manifestations in models C to E without reference to the observed spectrum. Finally, we test models that look acceptable by comparing them with spectra obtained with two different samples at room temperature on two different spectrometers (see Experimental).

Model A

Geometric Analysis

The nth-nearest cation neighbors of a cation M_0 in a structure of the NaCl type are at distances $d_{0,n} = a(n/2)^{1/2}$Å. The cation coordinations of M_0 in cubic $LiFeO_2$ up to $n = 8$ are listed in Table I. The six O_1 atoms at 2.08 Å completely shield the six M_2 cations from M_0. The 24 M_3 cations are at the relatively long distance of 5.09 Å from M_0, but at the shortest distances $d_{3,3} = 2.94$ Å from one another; there is a high probability that the Li^{1+} and Fe^{3+} ions will be distributed more or less uniformly among the vertices of the coordination rhombicuboctahedron, thereby reducing the effect of the M_3 cation shell on the symmetry of the electric field at M_0.[1] Assuming that the dominant contribution of cation neighbors to the asymmetry of the field at $M_0 = Fe_0$ comes from the 12 M_1 cations, the

[1] The species $Li_{24-k}Fe_k$, $10 \leq k \leq 14$, account for about 70% of the possible occupancies of the vertices of the rhombicuboctahedron by Li and Fe atoms. The number of distinct (up to rotation and reflection) configurations on the rhombicuboctahedron is 41 278 each for $k = 10$ and 14, 52 234 each for $k = 11$ and 13, and 56 846 for $k = 12$ (*2, 3*).

TABLE I

CATION COORDINATION OF A CATION M_0 IN CUBIC $LiFeO_2$[a]

Cations	Coordination figure	$d_{0,n}$ (Å)	$d_{n,n}$ (Å)	$\sum_1^n M_i$
12 M_1	Cuboctahedron	2.94	2.94	12
6 M_2	Octahedron	4.16	5.88	18
24 M_3	Rhombicuboctahedron	5.09	2.94, 4.16	42
12 M_4	Cuboctahedron	5.88	5.88	54
24 M_5	Truncated octahedron	6.57	2.94, 5.88	78
8 M_6	Cube	7.20	8.31	86
48 M_7	Truncated cuboctahedron	7.77	2.94, 4.16, 5.09	134
6 M_8	Octahedron	8.31	11.75	140

[a] All atoms are at points of an idealized rigid NaCl-type lattice; $d_{0,n}$, M_0–M_n distance; $d_{n,n}$, shortest M_n–M_n distances in the coordination polyhedron; $\sum_1^n M_i$, total number of cation neighbors of M_0 within, and including, $d_{0,n}$.

TABLE II

COORDINATES (IN Å) OF THE VERTICES OF THE NORMALIZED CUBOCTAHEDRON AND CONTRIBUTIONS TO THE ELECTRIC-FIELD GRADIENT TENSOR EFG FROM UNIT CHARGES AT THE VERTICES

				$V^0(s) = u^{-1} r^5 V(s)$					
Vertex s	x	y	z	xx	yy	zz	xy	xz	yz
a	1	0	1	1	−2	1	0	3	0
b	0	1	1	−2	1	1	0	0	3
c	−1	0	1	1	−2	1	0	−3	0
d	0	−1	1	−2	1	1	0	0	−3
e	1	1	0	1	1	−2	3	0	0
f	−1	1	0	1	1	−2	−3	0	0
g	−1	−1	0	1	1	−2	3	0	0
h	1	−1	0	1	1	−2	−3	0	0
i	1	0	−1	1	−2	1	0	−3	0
j	0	1	−1	−2	1	1	0	0	−3
k	−1	0	−1	1	−2	1	0	3	0
m	0	−1	−1	−2	1	1	0	0	3

TABLE III

DISTINCT $Li_{12-k}Fe_k$ CONFIGURATIONS $\mathscr{C}$, $0 \le k \le 5$, ON A CUBOCTAHEDRON, THEIR SYMMETRIES AND ORIENTATIONAL MULTIPLICITIES p[a]

$\mathscr{C}$	Symmetry	p	$\mathscr{C}$	Symmetry	p	$\mathscr{C}$	Symmetry	p
	$\underline{k=0}$		*abce*	1	48	*abcfi*	1	48
Li_{12}	$m3m$	1	*abcg*	1	48	*abcjk*	1	48
	$\underline{k=1}$		*abcj*	m_a	24	*abdej*	m_d	24
a	$m_a m_d$	12	*abck*	1	48	*abdfg*	m_a	24
	$\underline{k=2}$		*abcm*	m_a	24	*abdgj*	1	48
ab	m_d	24	*abeg*	m_d	24	*abdgk*	1	48
ac	$m_a m_a$	12	*abfi*	1	48	*abdgm*	2_d	24
af	2_d	24	*abfk*	m_d	24	*abdik*	m_a	24
ak	$m_a m_d m_d$	6	*abfm*	2_d	24	*abdjm*	m_a	24
	$\underline{k=3}$		*abgj*	1	48	*abefk*	1	48
abc	m_a	24	*abgk*	2_d	24	*abefm*	1	48
abe	$3m_d$	8	*abij*	$m_a m_d$	12	*abehj*	1	48
abf	2_d	24	*abjk*	2_a	24	*abekm*	m_d	24
abg	m_d	24	*abjm*	1	48	*abfgh*	m_d	24
abj	1	48	*abkm*	$2_d/m_d$	12	*abghj*	2_d	24
abk	1	48	*acik*	$\bar{4}/m_a m_a m_a$	3	*abgim*	1	48
acj	m_a	24	*acjm*	$\bar{4}2_d m_a$	6	*acefm*	$m_a m_d$	12
ack	$m_a m_d$	12		$\underline{k=5}$		*acegi*	1	48
afm	32_d	8	*abcde*	m_d	24	*acehm*	1	48
	$\underline{k=4}$		*abcdj*	m_a	24	*achjk*	2_d	24
abcd	$4m_a m_d$	6	*abcef*	$m_a m_d$	12	*adegk*	2_d	24

[a] The vertices specified under $\mathscr{C}$ are occupied by Fe in the compositions $Li_{12-k}Fe_k$ and by Li in the complementary compositions Li_kFe_{12-k}; for Li_6Fe_6, see Table IV. Symmetry elements: m_a, axial mirror plane; m_d, diagonal mirror plane; 2_a, axial digyre (subgroup of a tetragyre); 2_d, diagonal digyre.

analysis may be restricted, in the first approximation, to the M_1 cuboctahedron (Table II).

The M_1 cuboctahedron shells have compositions $Li_{12-k}Fe_k$ whose frequencies of occurrence will be distributed symmetrically about the peak frequency at $k = 6$. With the exception of $k = 0$ and 12, none of the Li,Fe configurations on these cuboctahedra are of cubic symmetry. To obtain an idea of the distribution of the EFG at Fe_0 it is necessary to enumerate all the distinct Li,Fe configurations for each k. A distinct configuration is unique up to rotation and reflection; the total number of its orientations in the structure and mirror images is given by the orientational multiplicity p.

Application of Pólya's theorem to substitution on a cuboctahedron of symmetry $m3m$ shows (*2*) the numbers $N(k)$ of such configurations $\mathscr{C}$ to be $N(0) = 1$, $N(1) = 1$, $N(2) = 4$, $N(3) = 9$, $N(4) = 18$, $N(5) = 24$, and $N(6) = 30$; $N(12 - k) = N(k)$. The configurations $\mathscr{C}$ for $0 \leq k \leq 6$ are enumerated in Tables III and IV, together with their symmetries and orientational multiplicities. The remaining, "complementary," configurations $\mathscr{C}^*$ ($k > 6$) are obtained by interchanging Li and Fe.

The case of $k = 6$ requires comment. The set of 30 distinct configurations of the Li_6Fe_6 variety (Table IV) *already* contains all the complementary pairs that can be produced by interchanging Li and Fe. Moreover, 8 of the 30 configurations are self-complementary (i.e., each is its own complement), and 3 of the 8 are self-dual, i.e., self-complementary with respect to inversion in M_0 (cf. Refs. (*4*, *5*)). Thus the total number of all possible distinct $Li_{12-k}Fe_k$ configurations for $0 \leq k \leq 12$ is 144.

TABLE IV

DISTINCT Li_6Fe_6 CONFIGURATIONS ON A CUBOCTAHEDRON, THEIR SYMMETRIES AND ORIENTATIONAL MULTIPLICITIES p[a]

$\mathscr{C}$	Symmetry[b]	p	$\mathscr{C}^*$
abcdef	$\underline{2}'/m \mid m_a$	24	SD
abcdeg	$\underline{4}'\,2'\,m \mid m_d\,m_d$	12	SC
abcdej	1	48	*abcefg*
abcdek	1	48	*abdefg*
abcdij	m_d	24	*abcfik*
abcdjm	$m_a\,m_a$	12	*abdijm*
abcefm	$m_a\,m_d$	12	*abdfgk*
abcegi	1	48	*abcegk*
abcegm	$\underline{2}' \mid 1$	48	SC
abcehj	$\underline{3}' \mid 3$	16	SD
abcehk	1	48	*abchij*
abcehm	$2' \mid 1$	48	SC
abcghj	$2'/m \mid m_a$	24	SD
abcgik	2_d	24	*abdijk*
abdfkm	1	48	*abeghk*
abdgkm	1	48	*abfjkm*
abdjkm	$\underline{4}'/m \mid 2_a/m_a$	12	SC
abegkm	$\underline{3}m_d$	4	*abfhkm*
acfhjm	$4'\,22 \mid 2_a\,2_d\,2_d$	12	SC

[a] Notation as in Table III. SC, self-complementary; SD, self-dual (see text).

[b] For the SC and SD configurations both the dichromatic point group **G** and its maximal monochromatic subgroup **M** are shown, **G** | **M** (cf. Ref. (*4*)).

Distribution of EFG Values

If a formal charge of +2 is assigned to all cations other than M_1, the only charges u that can produce a nonzero EFG at $Fe_0(000)$ are those on M_1. In this model the local asymmetry manifests itself, not metrically, but only as the effect, at Fe_0, of the difference in the formal cation charges on an undistorted cubic lattice.

The EFG tensor appropriate to the cuboctahedron is

$$\mathbf{EFG} = -\begin{pmatrix} \Sigma V_{xx} & \Sigma V_{xy} & \Sigma V_{xz} \\ \Sigma V_{xy} & \Sigma V_{yy} & \Sigma V_{yz} \\ \Sigma V_{xz} & \Sigma V_{yz} & \Sigma V_{zz} \end{pmatrix},$$

tr **EFG** = 0, where $V_{xx} = u(3x^2 - r^2)/r^5$, etc.; $V_{xy} = 3uxy/r^5$, etc.; $r^2 = x^2 + y^2 + z^2$; and the summation is over the 12 sites (Table II). Only two of the three eigenvalues v of this symmetric tensor, $|v_{zz}| \geq |v_{yy}| \geq |v_{xx}|$, are needed to define EFG, as $\mathrm{EFG} = v_{zz}\,(1 + \eta^2/3)^{1/2}$, $\eta = (v_{yy} - v_{xx})/v_{zz}$, and $v_{xx} + v_{yy} + v_{zz} = 0$. For an axial EFG ($v_{xx} = v_{yy}$), $\mathrm{EFG} = v_{zz}$. When $v_{zz} = -v_{yy}$, $|\mathrm{EFG}| = (2/3^{1/2})|v_{zz}|$, but the sign of EFG is indeterminate. This is possible only when det **EFG** = 0 and in fact only when $k = 0 \pmod 3$ (see Appendix). The $v_{zz}^2 = (\Sigma V_{xy})^2$

TABLE V

SYMMETRY WITH RESPECT TO EFG OF DISTINCT $Li_{12-k}Fe_k$ CONFIGURATIONS AND THEIR EFG VALUES AND |EFG| FREQUENCIES

Configuration[a]	Symmetry	−EFG[b]	Frequency
abegkm	$\bar{3}m_d$	$+(18)^{1/2}$	8
*abkm; abekm, adegk**	$2_d/m_d$ (3×)	$+(14)^{1/2}$	120
abcegm (SC), *abdjkm* (SC)	$\underline{2}_d/m_d$, $2_a/m_a$	$(12)^{1/2}$	60
acegi	$\underline{1}$	$+(11)^{1/2}$	96
abcegi, abdfkm, abdgkm	$\bar{1}$ (3×)	$+(10.5)^{1/2}$	288
abeg, abfk, abfm*, abgk*	$\underline{2}_d/m_d$ (4×)	$+(9.5)^{1/2}$	192
abk	$\bar{1}$	$+9^{1/2}$	96
ak; abcm, abjk, acik; abdgk, abdjm*, abefk, abefm, abgim*	$m_a\,m_d\,m_d$; $2_a/m_a$ (2×), $4/m_a\,m_a\,m_a$; $\bar{1}$, $2_a/m_a$, $\bar{1}$ (3×)	$+8^{1/2}$	546
abcdij, abcgik	$2_d/m_d$ (2×)	$+(7.5)^{1/2}$	96
abck, abjm; abcfi, abdej, abdgj*, abdgm, abfgh*, achjk*	$\bar{1}$ (2×); $2_d/m_d$ (6×)	$+(6.5)^{1/2}$	576
ack, ack; abcdeg* (SC), *abcdjm, abcdjm*, abcefm, abcefm*, abcehm* (SC), *acfhjm* (SC)	$m_a\,m_d\,m_d$ (9×)	$6^{1/2}$	144
abcdj, abcjk, abdik	$\underline{2}_a/m_a$ (3×)	$+5^{1/2}$	192
abcdej, abcdej, abcdek, abcdek*, abcehk, abcehk**	$\underline{1}$ (6×)	$(4.5)^{1/2}$	416
abe, abf, abg, afm**	$\bar{3}m_d$ (4×)	$+(4.5)^{1/2}$	
ab, af; abce, abcg*, abfi*, abgj**	$2_d/m_d$ (6×)	$+(3.5)^{1/2}$	480
abc, abc, abj, abj*, acj, acj**	$2_a/m_a$ (6×)	$3^{1/2}$	192
a; ac; abcd, abcj, abij, acjm; abcde*, abcef*, abdfg*, abehj*, abghj*, acefm*, acehm**	$m_a\,m_d\,m_d$ (2×), $4/m_a\,m_a\,m_a$ (4×), $m_a\,m_d\,m_d$ (7×)	$+2^{1/2}$	528
Li_{12}, Fe_{12}; *abcdef* (SD), *abcehj* (SD), *abcghj* (SD)	*m*3*m* (5×)	0	66

[a] Configuration *adegk** (Li_5Fe_7) is complementary to configuration *adegk* (Li_7Fe_5) with respect to interchange of Li and Fe, etc. SC, self-complementary; SD, self-dual.

[b] In Å^{-3} (referred to the normalized cuboctahedron of Table II). Because of EFG($\mathscr{C}$) = −EFG($\mathscr{C}^*$), only configurations giving negative values of EFG are listed. Where no sign is indicated the sign of EFG is indeterminate (see text); in that case *all* the configurations yielding the same |EFG| are listed.

$+ (\Sigma V_{xz})^2 + (\Sigma V_{yz})^2 + (\Sigma V_{xx})^2 + (\Sigma V_{xx})(\Sigma V_{yy}) + (\Sigma V_{yy})^2$.

Because of the invariance of V_{xx}, V_{xy}, etc., with respect to inversion of the vertices about the center of the cuboctahedron, only 17 distinct |EFG| values, including zero, correspond to the 144 distinct configurations $\mathscr{C}$ (Table V and Fig. 1). For example, the charge pairs $a^{+1}k^{+3}$ and $a^{+3}k^{+1}$ produce identical **EFG** and can both be replaced by the EFG-equivalent pair $a^{+2}k^{+2}$. This means that all centrosymmetric 1–3 charge pairs can be replaced by equivalent, "neutral," 2–2 pairs, so that the symmetry G(**EFG**) of a configuration relative to **EFG**, and its |EFG| equivalence, are determined by the 1–1 and 3–3 pairs. For centrosymmetric configurations the point-group symmetries G(**EFG**) and $G(\mathscr{C})$ are identical, but for noncentrosymmetric configurations G(**EFG**) is at least $G(\mathscr{C}) \times \bar{1}$ and in some cases higher.[2]

Since replacement of a +1 charge by +3 at a vertex s in Li_{12} changes ΣV_{xx}, ΣV_{yy}, etc., of the **EFG** matrix from zero to $2V_{xx}(s)$, $2V_{yy}(s)$, etc., respectively, replacement of a +3 charge in Fe_{12} by +1 produces $\Sigma V_{xx} = -2V_{xx}(s)$, etc. (cf. Appendix). Consequently EFG($\mathscr{C}$) = −EFG($\mathscr{C}^*$); i.e., the EFG distribution is symmetric about zero. The frequencies of occur-

[2] Thus G(**EFG**) = *m*3*m* can result from $G(\mathscr{C})$ = 3 or *m*; $\bar{3}m$ from 2 or *m*; 4/*mmm* from *mm* or *m*; *mmm* from *m*, 2, or 1; and 2/*m* from 1.

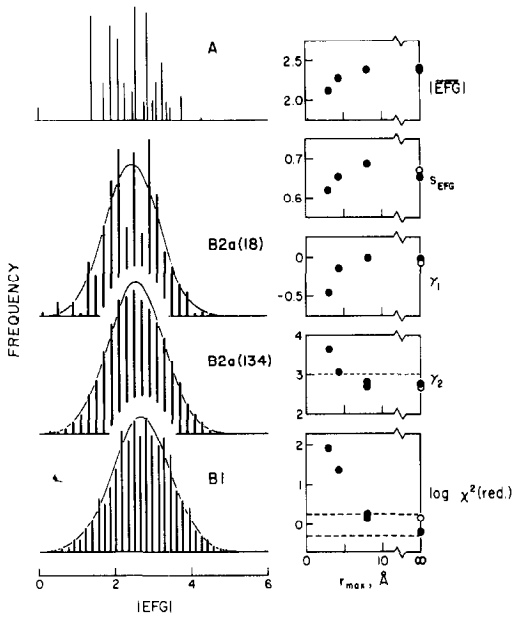

FIG. 1. Distribution of |EFG| values in models A and B and the normal curves fitted to these distributions (for symbols, see Table VI). For a normal distribution, $\gamma_1 = 0$ and $\gamma_2 = 3$. The 5 to 95% limits of the χ^2(red.) distribution are indicated by dashed lines. The open circles refer to sample B1.

rence of the |EFG| values in the set of $\sum_1^{144} p_i(\mathscr{C}_i) = 2^{12} = 4096$ configurations are given in Table V, and the distribution is plotted in Fig. 1. The |EFG| distribution, which of course is exact and not a sampling distribution, would translate into a simulated spectrum already containing, the restrictive nature of model A notwithstanding, the gross features of the observed spectrum, viz., a symmetric doublet with broadened, somewhat asymmetric components; this result is considered in more detail in a subsequent section. The weighted mean of the |EFG| distribution is 2.378 when referred to the normalized cuboctahedron of Table II, and 2.114 when referred to $\frac{1}{2}a$.

Apart from the varieties Li_{12} and Fe_{12}, both of symmetry $m3m$, three other configurations give zero values of EFG. These are the self-dual configurations *abcdef*, *abcehj*, and *abcghj*. Although their symmetries are not cubic, their EFG values are zero for the following reason. Because these configurations are self-dual, they differ from their respective complementary configurations only by their relative orientations or chiralities, i.e., they are congruent with respect to rotation or reflection and are thus identical relative to EFG. But $EFG(\mathscr{C}) = -EFG(\mathscr{C}^*)$; hence $EFG = 0$.[3]

Model B

Extension of the exact geometric analysis to include second-nearest cation neighbors M_2 entails enlarging the M_1 cuboctahedron to an $M_1 + M_2$ coordination figure of 18 vertices, which is a cuboctahedron augmented on its square faces (= "cuboctahedron + 6," polyhedron **18-3** of Ref. (*2*)). The number of distinct $Li_{18-k}Fe_k$ configurations on this polyhedron is 6456 (Table 15 of Ref. (*2*)) compared with 144 $Li_{12-k}Fe_k$ configurations on the cuboctahedron. Construction of such a number of configurations, and elimination of duplicates, would constitute a very large effort even with the aid of a computer. Extension to $M_1 + M_2 + M_3$ environments would require computing the EFG values due to 91 633 094 080 distinct $Li_{42-k}Fe_k$ configurations which would first have to be constructed (cf. Refs. (*2*, *3*) for method of enumeration). Geometric analysis is then clearly an impossible task even for cation environments restricted to only the first three cation shells, and direct computer simulation must be resorted to if the effect of more distant cations on the |EFG| distribution is to be investigated.

In choosing sample size it was necessary to compromise between high statistics and the necessity of keeping the computing effort small. Although the samples described in the following were thought to be of reasonable size, it is well to keep in mind that the population of the cation environments being sampled is very large.

[3] A detailed treatment of charge configurations having zero EFG is found in Refs. (*4*, *5*).

TABLE VI

PARAMETERS OF |EFG| DISTRIBUTIONS FOR VARIOUS MODELS AND SAMPLES[a]

Model and sample	$\|\overline{EFG}\|$	s_{EFG}	γ_1	γ_2	χ^2(red.)
A	2.114(10)	0.621	−0.46	3.66	80.7
B1	2.38(2)	0.67	−0.07(6)	2.66(11)	1.4
B2a(18)	2.19(2)	0.63	−0.16(4)	3.04(8)	24.2
B2a(134)	2.28(2)	0.69	0.01(4)	2.68(8)	1.3
B2b(134)	2.28(1)	0.69	0.03(3)	2.80(6)	1.7
B2a(∞)	2.28(2)	0.65	−0.02(4)	2.74(8)	0.6
C2b(134; 2%)	1.96(1)	0.61	0.12(3)	2.82(6)	1.8
C2b(134; 5%)	1.68(1)	0.66	0.53(3)	3.10(6)	18.1
C2b(134; 10%)	2.39(2)	0.87	0.32(3)	2.77(6)	7.3
C2b(134; 15%)	4.10(2)	1.28	0.07(3)	2.69(6)	2.3
D2b(134; −1, −2)	2.34(1)	0.79	0.22(3)	2.80(6)	3.9
E2b(134; −1, −2; 2%)	2.15(1)	0.74	0.28(3)	2.81(6)	5.8
E2b(134; −1, −2; 5%)	2.01(1)	0.78	0.50(3)	3.08(6)	15.3
E2b(134; −1, −2; 8%)	2.14(2)	0.91	0.56(3)	2.97(6)	19.1
E2b(134; −1, −2; 10%)	2.40(2)	0.97	0.52(3)	2.92(6)	14.6
E2b(134; −1, −0.1; 5%)	2.08(1)	0.74	0.40(3)	2.99(6)	9.1
E2b(134; −1, −0.5; 5%)	2.07(1)	0.73	0.45(3)	2.96(6)	12.8
E2b(134; −1, −1; 5%)	2.07(1)	0.79	0.44(3)	2.87(6)	12.8
E2b(134; −1, −2.5; 5%)	2.01(1)	0.75	0.49(3)	2.98(6)	15.4

[a] $|\overline{EFG}| = |EFG|$ mean; s_{EFG} = standard deviation; $\gamma_1 = m_3 m_2^{-3/2}$ = moment coefficient of skewness; $\gamma_2 = m_4 m_2^{-2}$ = moment coefficient of kurtosis; χ^2(red.) = χ^2/(no. of degrees of freedom), goodness of fit to a normal distribution having the same mean and s_{EFG}.

Sample B1

The reference site M_0 was at the center of a block of 6 × 6 × 6 unit cells, i.e. a block 24.9 Å on edge and ca. 1.55 × 10^4 Å^3 in volume. The sample included cation sites in the boundaries of the block, totaling 1098 cations contributing to the EFG at M_0. Thus *all* 458 cations within $r_{max} \leq d_{0,17} \approx 12.47$ Å were included in the EFG summation, *plus* 640 of the 1888 cations contained between spherical surfaces of $r = 12.7$ and 21.6 Å, i.e., $d_{0,18} \leq r \leq d_{0,36}$. The 1098 cation sites were assigned +1 and +3 charges at random and the EFG was computed. This was repeated 2025 times. The parameters of the resulting |EFG| distribution (Fig. 1) are listed in Table VI.

Sample B2

A trial sample B2a of 12 × 12 × 12 unit cells, corresponding to a volume of about 1.24 × 10^5 Å^3, was first set up to determine the smallest r_{max} that would yield a reasonable approximation to the limiting EFG distribution without the expenditure of excessive computer time. This sample contained a total of 13 824 sites, of which 3474 were Fe sites. The |EFG| distribution for $r_{max} = 0.75a < d_{0,2}$ agreed well with model A. Increasing r_{max} successively to $1.05a < d_{0,3}$ (18 cation neighbors, B2a(18)) and $1.9a < d_{0,8}$ (134 cation neighbors, B2a (134)) revealed the inadequacy of model A and a tendency toward a normal distribution (Fig. 1 and Table VI). Statistical comparison showed that the |EFG| distributions from B1 and B2a(134) were closely similar to the symmetric, slightly platykurtic "limiting" distribution B2a(∞) described in Experimental. Thus taking $r_{max} = 1.9a$ will furnish a reasonable approximation, within the sample statistics, to the limiting distribution for model B without excessive computation.

A larger sample B2b (15 × 15 × 15 unit cells, ≈2.42 × 10^5 Å^3 in volume, containing

6742 Fe sites in a total of 27 000 lattice sites) was then generated for use in the refined EFG computations (models C to E). The |EFG| distribution for $r_{max} = 1.9a$, B2b(134), was statistically indistinguishable from B2a(134), which confirms that in the random samples cations beyond M_7 contributed only marginally to the EFG distribution. The |EFG| mean for the set B1, B2a(134), B2a(∞), and B2b(134) was about 9% higher than the $|\overline{EFG}|$ of model A.

It is interesting to note that in model A, 66/4096, or approximately 1.6%, of the cuboctahedral cation environments of Fe atoms produce zero EFG at their reference sites; in sample B2a(18), about 0.3% of the |EFG| values fall within the 0 to 0.2 interval. By contrast, in B1, B2a(134), B2a(∞), and B2b(134) the 0 to 0.2 interval is empty. This indicates the bias of the M_1 and $M_1 + M_2$ approximations and demonstrates the very rapid falloff in the fraction of distinct configurations having zero EFG:[4] for the M_1 configurations the fraction is 5/144 (≈3.5%), for the $M_1 + M_2$ configurations, 24/6456 (≈0.37%), and for the $M_1 + M_2 + M_3$ configurations, 55516/91 633 094 080 ($\approx 6.1 \times 10^{-5}$%), so that the fraction is completely negligible when cation neighbors beyond M_2 are included in the EFG summation. In an EFG($q_{val} = 0$) distribution for an equimolar binary ionic solid solution the frequency of the EFG = 0 component is therefore always practically zero.

Model C

The anion locations within the computer were coded with displacements of one unit (=d) toward each of the nearest Fe atoms. The direction of this displacement is consistent with the larger effective ionic radius of Li^{1+}: $r^{vi}(Li^{1+}) = 0.76$ Å, $r^{vi}(Fe^{3+}_{HS}) = 0.645$ Å (*6*). It is also the direction in which oxygen atoms are displaced in the ordered tetragonal $LiFeO_2$ phase γ (or Q_1) (*1*), and there is evidence (*7*) that such a displacement actually occurs in α-$LiFeO_2$.

Considering that the reference nucleus M_0 in our EFG computations is always Fe, i.e., cation of the higher charge, the six O_1 atoms would all be displaced by equal amounts toward Fe_0 if it were not for the compensating effect of Fe atoms at $d_{0,1}$ and beyond. In this sense the displacement of an O_1 in the computer simulation reflects the cation distribution in the more distant environment of Fe_0.

The |EFG| distributions C2b obtained by displacing the oxygen atoms in sample B2b by d ranging from 2 to 15% of the equilibrium interatomic distance Fe–O = $\frac{1}{2}a$ (i.e., by 0.04 to 0.31 Å parallel to a crystallographic axis) and setting $r_{max} = 1.9a$ are shown in Fig. 2, and their parameters are listed in Table VI and plotted in Fig. 3. Similar computations were also carried out for sample B2a; the parameters of the resulting distributions were consistent with those for the C2b set (Fig. 3).

The $|\overline{EFG}|$ value varied with the oxygen displacement. attaining a minimum at d

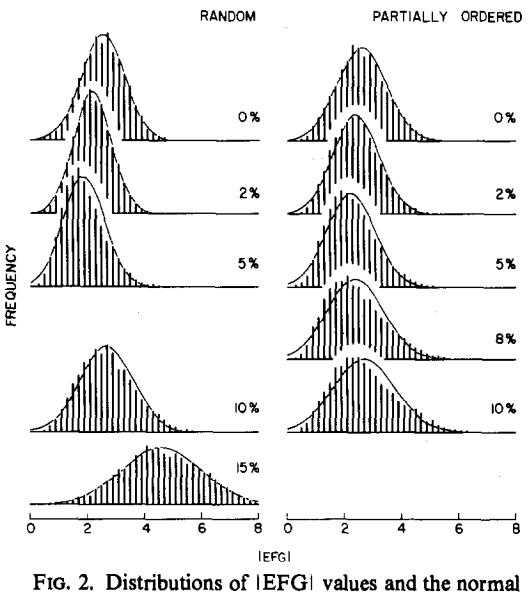

FIG. 2. Distributions of |EFG| values and the normal curves fitted to these distributions. Left, random samples B2b(134; 0%) and C2b(134; 2 to 15%). Right, partially ordered samples D2b(134; 0%) and E2b(134; −1, −2; 2 to 10%).

[4] On a cubic lattice these configurations are self-dual. They and their enumeration are discussed in detail in Ref. (*4*).

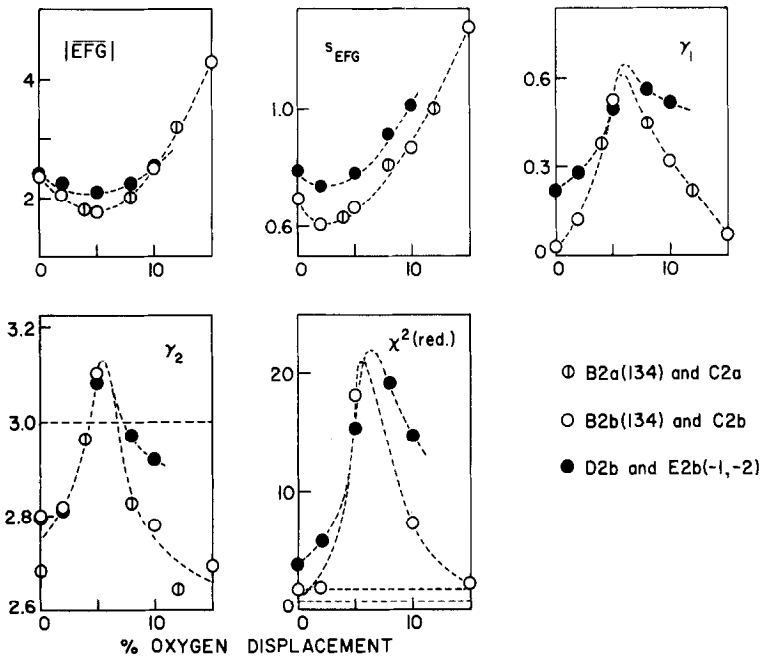

FIG. 3. Parameters of the |EFG| distributions of Fig. 2 (see caption of Fig. 1).

between 5 and 6% (0.10 to 0.13 Å) and then rising steadily with further displacement. The other parameters paralleled the variation of the mean. In particular, the moment coefficient of skewness, γ_1, was appreciable at ≈6% displacement, whereas at 2 and 15% it was close to zero. The moment coefficient of kurtosis, γ_2, showed that the distribution was platykurtic ($\gamma_2 < 3$) at 2 and 15% displacement but slightly leptokurtic ($\gamma_2 > 3$) at 6%.

When the C2b distributions are fitted to normal distributions having the same means and standard deviations, the χ^2(red.) = χ^2/(no. of degrees of freedom) value, which almost falls within the 5 to 95% interval of the χ^2(red.) distribution at 0% displacement in B2b(134), increases sharply to a maximum at ≈6% displacement and tends to return to the acceptable χ^2(red.) range as the amount of displacement increases further (Fig. 3).

Model D

There is evidence (*1*, *7–9*) that quenching of $LiFeO_2$ from high temperatures does not produce structures that are entirely random in Fe and Li. The values (±0.02) of the short-range order parameters s_l of samples quenched from 857 and 742°C, respectively, were estimated by Brunel and de Bergevin (*7*, *8*) from X-ray powder diffraction data as

	s_1	s_2	s_3	s_4	s_5
857°C	0.15	0.19	−0.07	0.01	−0.08
742°C	0.16	0.23	−0.05	0.01	−0.06

$s_l = 2p_l - 1$, where p_l is the probability of finding a Li atom at a distance r_l from an Fe atom.

To take the incipient short-range ordering into account the Fe and Li atoms in sample B2b were shuffled to give, approximately, the observed values of s_l. The shuffling was accomplished by introducing a repulsive potential $E_{0,n}$ between Fe atoms and progressing toward minimization of the total repulsive energy until the desired approximation to the observed values of s_l had been achieved (Fig. 4).

Setting $E_{0,1} = -1$ and $E_{0,2} = -2$ gave $s_1 = 0.21$, $s_2 = 0.24$, $s_3 = 0.10$, $s_4 = 0.09$, $s_5 = 0.07$.

These values were considered sufficiently close to Brunel and de Bergevin's estimate. The |EFG| distribution for $r_{max} = 1.9a$, D2b(134; −1, −2) (Fig. 2 and Table VI), resembles most closely the distribution C2b(134, 10%); like it, it is positively skew and its mean is displaced toward higher values relative to B2b(134).

The reason for the positive skewness is the asymmetry about zero of the corresponding EFG distributions, the cause of which in turn is to be sought in the depletion of positive charge in the M_1 environments of the Fe atoms. On introduction of the Fe–Fe repulsive potential there will be, on the average, fewer +3 charges around an Fe atom and more +3 charges around a Li atom, but the EFG at the Li sites is not probed, hence the |EFG| distribution for the Fe sites contains a smaller proportion of contributions from environments with Fe > Li. This asymmetry does not seem to affect $|\overline{EFG}|$ appreciably, but it is reflected in γ_1. The |EFG| distribution for model A serves to demonstrate this tendency to positive skewness, for the major contribution to the distributions including cations beyond M_1 comes from the 12 nearest cation neighbors. When the contributions of all $Li_{12-k}Fe_k$ configurations with $k \geq 6$ are removed from the distributions for model A, $|\overline{EFG}|$ drops by about 2% but γ_1 becomes appreciably less negative; reinstating the configurations with $k = 6$ overcompensates in the opposite direction:

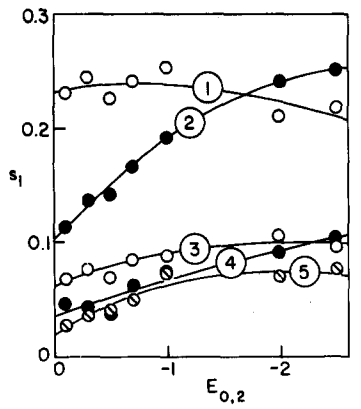

FIG. 4. The short-range order parameters s_i of |EFG| distributions produced in sample C2b(134; 5%) by introduction of repulsive energy $E_{0,1} = -1$ and $E_{0,2} = -0.1$ to −2.5 between Fe atoms (see text). Samples E2b(134; −1, $E_{0,2}$; 5%).

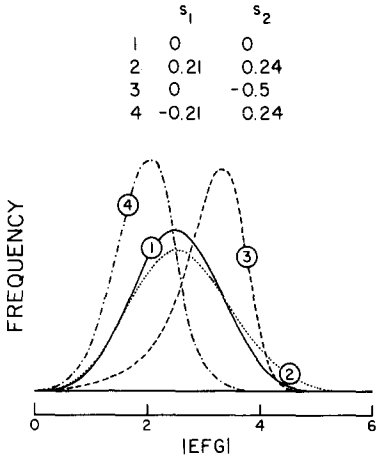

FIG. 5. Illustration of the effect of short-range ordering on the |EFG| distribution, at 0% oxygen displacement. Curve 1, sample B2b(134); curve 2, sample D2b(134; −1, −2).

	A (all k)	$k < 6$	$k \leq 6$
$\|\overline{EFG}\|$	2.114	2.069	2.108
s_{EFG}	0.621	0.529	0.635
γ_1	−0.46	−0.20	−0.76
γ_2	3.66	2.09	4.26

The changes in the |EFG| distribution that are produced in B2b by other types of short-range ordering are illustrated in Fig. 5.

Model E

The effect, on the |EFG| distribution, of simultaneously introducing short-range order and oxygen displacement (samples E2b(134)) is seen in Figs. 2 and 3 and in Table VI. Displacing the oxygen atoms in sample D2b(134; −1, −2) produced trends paralleling those obtained with the C2b(134) samples (Figs. 2 and 3). The $|\overline{EFG}|$ values in the 0 to 10% displacement range were somewhat higher and the s_{EFG} were significantly larger than the values in the C2b(134) series; the skewness was on the whole more pronounced.

The E2b(134; −1, −2) distributions all deviated significantly from normality.

Fixing the oxygen displacement at 5% and varying the degree of short-range order produced the E2b(134; −1, $E_{0,2}$; 5%) distributions listed in Table VI. The variation in the parameters of these distributions is largely due to the variation in s_2. The trends in this series were confused. The $|\overline{EFG}|$ was practically constant, while s_{EFG}, γ_1, and χ^2(red.) increased with s_2, although this correlation was not very strong.

Comparison with the Observed Spectrum

To clarify the relationship between an |EFG| distribution and the Mössbauer spectrum, let us consider how a model |EFG| distribution is converted into a simulated spectrum. A symmetric Lorentzian doublet is assigned to each component of the distribution (actually the $|g|$ distribution; see below). The separation of the two components of each doublet is proportional to the particular |EFG| value, and the intensity of each doublet is proportional to the frequency of the |EFG| value; the doublets have identical preassigned half-widths and are assumed centered at the same point of the velocity scale, the (mean) ^{57}Fe isomer shift in the crystal. The simulated spectrum is obtained by summing over the Lorentzians at each value of the |EFG| distribution; the separation of the centroids of the two symmetric halves of the spectrum corresponds to $|\overline{\Delta}|$, to be compared with $|\Delta_{obs}|$. In the continuous |EFG| limit the spectrum corresponds to a convolution of the |EFG| (density) function with a Lorentzian function.

The room-temperature spectrum of polycrystalline α-$LiFeO_2$ (quenched from 900°C) reported by Cox *et al.* is a partially resolved doublet with broadened lines (Fig. 8a of Ref. (*1*)), as were our own high-statistics spectra recorded on the Exeter (EX) and Aberdeen (AB) spectrometers. That the spectrum is not a *simple* Lorentzian doublet was established by fitting two unconstrained single Lorentzians to EX and AB. For the number of degrees of freedom involved the 5 to 95% limits of the χ^2 distribution would require values between 135 and 258 for EX, and between 308 and 484 for AB. However, the unacceptable χ^2 values of 1526 for EX and 4694 for AB were obtained; the value for EX was reduced to 935 when two Voigt functions were used instead of two Lorentzians.

It is clear that any of the models A to E would yield a symmetric doublet and that even the simplest model, A, would account, qualitatively, for the observed spectrum. To examine the validity of the model in detail we should (1) extract a value of $|\Delta_{obs}|$ from the experimental spectrum and compare it with the $|\overline{\Delta}|$ value calculated from the mean of an |EFG| distribution, and (2) match the profiles of the observed and the simulated spectra.

In comparing the observed spectrum with the results for models C to E, it is always assumed that the $|\Delta_{obs}|$ and the shape of the observed spectrum arise principally from the lattice terms: the magnitude of the q_{val}, η_{val} contribution is not known, beyond the fact that $(1 - \gamma_\infty)/(1 - R) > 10$ and that $q_{val}(Fe^{3+}_{HS}) = 0$ for the ion in a cubic environment, and no attempt was made to estimate it.

Magnitude of the Quadrupole Splitting

The $|\Delta_{obs}|$ value corresponds to the separation, on the velocity scale, of the centroids of the components of the doublet. We assume that the mean $|\overline{EFG}|$ of an |EFG| *sampling*[5] distribution and the $|\overline{\Delta}|$ of the simulated spectrum are proportional and that $|\overline{EFG}|$ (Å^{-3}) $= K|\Delta_{obs}|$ (mm/sec). The success of the comparison will depend on how accurately we can evaluate K and how reliably we can determine the velocities corresponding to the two centroids.

The value of the conversion factor K depends on the values assumed for the ^{57}Fe

[5] The |EFG| distributions for models B to E (Table VI and figures) are sampling distributions; that for model A is an *exact* distribution, but it is treated, for the present purpose, as if it were a sampling distribution.

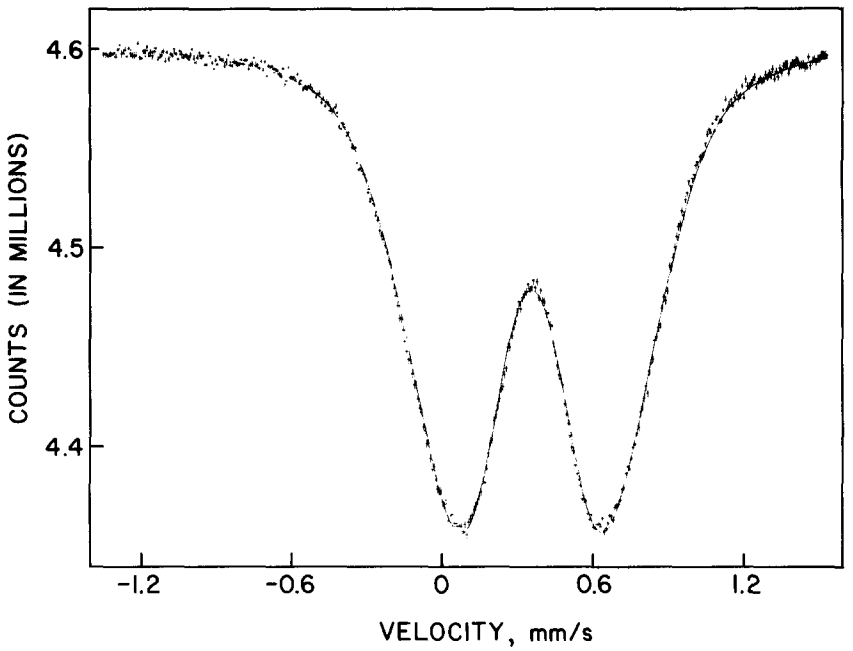

FIG. 6. The AB spectrum fitted to a spectrum simulated from the |EFG| distribution of sample C2a(134; 8%).

nuclear quadrupole moment Q and the Sternheimer antishielding factor γ_∞ (Eqs. (1)–(3)). If we take 0.19×10^{-24} cm^2 as the best estimate of Q, and γ_∞ as $-9.14(46)$ (*10*), remembering that the $|\overline{EFG}|$ are referred to $\frac{1}{2}a$ = 2.08 Å, then $K = 2.77$, with an estimated uncertainty of 20%.

Extraction of $|\Delta_{obs}|$ is not a trivial problem. The raw spectrum must be smoothed and corrected for the baseline, and the centroids of the "net" absorption must be computed, all in one computer-fitting operation. Since the fitting cannot be carried out unless the objective function is specified, and the $|g|$ distribution function underlying the observed spectrum is not known, we must find an empirical function that approximates the "net" absorption sufficiently closely for the centroids computed from it to be acceptable estimates of the centroids of the observed spectrum.

Fitting EX successively to i symmetric unconstrained Lorentzian doublets showed (*11*) that the area-weighted mean $\Sigma_i A_i|\Delta_i|/\Sigma_i A_i = |\Delta_{obs}|$ reached a practically constant value of 0.672(8) mm/sec after $i = 2$, and the χ^2 value was reduced to 305 for $i = 3$. This was the lowest χ^2 value obtained in any fitting of EX. While it is still not completely acceptable, it was considered that a fit to three unconstrained symmetric Lorentzian doublets described the observed spectrum adequately for the purpose of extracting $|\Delta_{obs}|$.

Fitting the denser AB spectrum (Fig. 6) to three symmetric Lorentzian doublets with all half-widths Γ contrained equal[6] resulted in the parameters listed in Table VII. The two-line spectrum, corrected for parabolic baseline, was highly symmetric ($\gamma_1 = 0.006$); its χ^2 was

TABLE VII

PARAMETERS OF THE ABERDEEN SPECTRUM

Lines	δ (mm/sec)	$\lvert\Delta\rvert$ (mm/sec)	Area (%)
1–2	0.364(4)	0.702(4)	38.6(6)
3–4	0.360(4)	1.001(4)	18.6(6)
5–6	0.365(3)	0.419(3)	42.8(10)
Mean[a]	0.364(8)	0.636(10)	

[a] Area-weighted (see text).

[6] Convergence could not be achieved without this constraint. The fitted half-width was 0.278(3) mm/sec.

TABLE VIII

FITTING THE OBSERVED ROOM-TEMPERATURE SPECTRA TO |EFG| DISTRIBUTIONS FOR MODEL C[a]

Sample	Spectrum EX			Spectrum AB		
	χ^2	χ^2(red.)	Γ(mm/sec)	χ^2	χ^2(red.)	Γ(mm/sec)
B2b(134; 0%)	720	3.75	0.34	1890	4.82	0.28
E2b(134; −1, −2; 5%)	440	2.29	0.30	873	2.22	0.24
E2b(134; −1, −2; 8%)	355	1.85	0.29	636	1.65	0.23
E2b(134; −1, −2; 10%)	524	2.73	0.30	679	1.73	0.24

[a] The 5 and 95% limits of the χ^2(red.) distribution correspond to about 0.7 to 1.34 for EX and about 0.8 to 1.24 for AB.

606. The difference of 0.036(9) mm/sec between $|\Delta_{obs}|$ of EX and AB is small considering that it represents the differences in the $LiFeO_2$ samples, the spectrometers, and the fitting procedure. Both $|\Delta_{obs}|$ values are slightly larger than the value quoted in Ref. (*1*), 0.56(5) mm/sec.

Converting $|\Delta_{obs}|$ to $|\bar{g}_{obs}| \approx |\overline{EFG}|_{obs}$ gave 1.76 and 1.86 Å^{-3}. The weighted mean, 1.8(5) Å^{-3}, is in reasonable agreement with all the model $|\overline{EFG}|$ values of Table VI except that for C2b(134; 15%). The point-charge model is thus seen to account qualitatively for $|\Delta_{obs}|$, but the large uncertainty in K (caused by the uncertainty of the Q value) does not allow us to decide which of the models is best without reference to the shape of the spectrum.

Shape of the Mössbauer Absorption

Fitting EX and AB to the 17 Lorentzian doublets required by model A, appropriately constrained, produced the unacceptable χ^2 values of 1246 for EX and 3535 for AB. The observed spectra were then fitted to spectra simulated from the |EFG| distributions for samples B2b(134) and E2b(134; −1, −2). Each point of the |EFG| sampling distribution was taken to give rise to a quadrupole doublet of splitting $\beta|EFG|$. The model function to be fitted was

$$y_c(v) = y_\infty[1 + BL(v_0 - v)^2]\{1 - \alpha\int_0^\infty [1/(1 + t_+^2) + 1/(1 + t_-^2)]f(|EFG|)d|EFG|\}, \quad (4)$$

where $t_\pm = (2/\Gamma)(\delta \pm \frac{1}{2}\beta|EFG| - v)$, $f(|EFG|)$ = frequency of |EFG|, Γ = linewidth, α = intensity, BL = fractional baseline curvature, v = velocity, v_0 = velocity at the center of the spectrum (channels), and y_∞ = baseline counts at the center of the spectrum in the absence of any resonant absorption. The integral was evaluated numerically by Simpson's rule. The results of the fitting are shown in Table VIII and Fig. 6.

The minimum of χ^2, or χ^2(red.), is seen to fall at about 8% oxygen displacement in both spectra. These χ^2 values are the lowest for any fit attempted except that to three unconstrained Lorentzian doublets. It is noteworthy that the 17-doublet fit, corresponding to model A, gave χ^2 values considerably larger than those obtained for the B2b(134; 0%) fit of Table VIII, which thus again shows the inadequacy of the nearest-neighbor-cations-only approximation.

An oxygen displacement of the order of 5% is not unreasonable. In γ-$LiFeO_2$, $\frac{1}{2}c$ = 4.37 Å = Fe–O + Li–O = 2.03 Å + 2.34 Å (*1*), which corresponds to a displacement of 0.15 Å ≈ 7% from the Fe–Li midpoint; a closely similar estimate, 2.035 Å, has been made (*7*) for the mean Fe–O distance in α-$LiFeO_2$ from diffuse X-ray scattering. An Fe–O distance of 2.03 Å in α-$LiFeO_2$ would correspond to ≈2½% displacement of the oxygen atom from its mean position if the Fe atom remained at its idealized lattice position.

Effect of Anion Polarization

The EFG experienced by any particular Fe nucleus is determined not only by the cation distribution but also by the displacement and polarization of the oxygen atoms. Anion polarization in α-$LiFeO_2$ has been estimated to contribute about 3% of the total electrostatic energy and seems to play an important part in the stabilization of the disordered phase (*7*, *12*).

Whereas models C and E take account of the cation distribution and oxygen displacement, to calculate the polarization would have meant, in addition to computing the EFGs, calculating the electric fields themselves by summing monopole and dipole contributions in a self-consistent manner. This was obviously impossible in terms of computer time, and so an explicit calculation of the effect of polarization was not made. However, an indication of the magnitude of this effect may be obtained from the following considerations.

In contrast to the disordered, almost cubic perovskites $Sr(Fe_{0.5}Ta_{0.5})O_3$ and $Pb(Fe_{0.5}Nb_{0.5})O_3$, in which the dominant contribution to the observed quadrupole splitting of 0.35–0.45 mm/sec at the Fe nucleus comes from oxygen polarization (*13*), in α-$LiFeO_2$ the effect of anion polarization on the EFG at Fe_0 must be smaller, perhaps appreciably so, than that of cationic disorder. This is seen, qualitatively, both from the difference in the geometries of the Fe environments in the two types of structure and, more directly, in the substantial measure of agreement between $|\bar{g}_{obs}|$ and the $|\overline{EFG}|$ values of Table VI (cf. also Fig. 6). In a mixed $ABO_3 = A^{2+}(Fe^{3+}_{0.5}M^{5+}_{0.5})O_3$ perovskite an Fe_0 atom is coordinated octahedrally by six oxygens at ca. 2 Å and six B atoms at ca. 4 Å with Fe_0–O–B collinear. If B = M, the oxygen atom is displaced toward M and polarized by it; if B = Fe, the oxygen, in the first approximation, remains at its lattice site and is not polarized. This coordination geometry corresponds to Fe_0–O_1–M_2 in α-$LiFeO_2$ except that O_1 moves toward Fe_0 if M_2 = Li and remains undisplaced if M_2 = Fe. In both structures the EFG at Fe_0 due to the oxygen atoms corresponds effectively only to fractional displacements of some of the −2 charges relative to the undisplaced (and unpolarized) −2 charges. In the perovskites the EFG at Fe_0 is thus due to contributions from the oxygens (displaced and polarized *away* from Fe_0) and from cationic disorder on the B sublattices; in α-$LiFeO_2$ the corresponding contributions are from O_1 (displaced and polarized *toward* Fe_0) and from cationic disorder at the M_2 sites. However, in α-$LiFeO_2$ a major contribution to the EFG at Fe_0 comes from the cationic disorder at the M_1 sites, at $1/2^{1/2}$ the Fe_0/M_2 distance from Fe_0 and involving a full charge difference of two units, whereas in the perovskite the nearest cation neighbors of Fe_0 are the A^{2+} atoms at $\frac{1}{2}a3^{1/2}$, and these are, in the first approximation, undisplaced and hence EFG-inactive.

With the exception of C2b(134; 15%), all the $|\overline{EFG}|$ values of Table VI are seen to be in the right range of $|\bar{g}_{obs}| \approx |\overline{EFG}|_{obs}$ if the uncertainty in K is taken into account. Since the conversion of $|\Delta_{obs}|$ to $|\bar{g}_{obs}|$ is not model dependent, this means that the model $|\overline{EFG}|$ essentially agrees with the $|\bar{g}_{obs}|$ even when the displacement and polarization of the oxygen atoms are completely neglected, as in model A. The effect of the oxygen displacement reduces the $|\overline{EFG}|$ of B2b(134) by a maximum of ca. 25% (in C2b(134; 5%)), i.e., to the estimated lower limit of the uncertainty in K, whereas in the E2b series the decrease is appreciably smaller. It would thus appear that the effect of polarization is within the uncertainty introduced with the present unreliable value of Q.

An additional effect is due to covalency. Since $LiFeO_2$ is not purely ionic, covalency will reduce the formal charges on the ions and consequently also q_{latt} and $|\Delta|$, and for the Fe^{3+}_{HS} ions in α-$LiFeO_2$, which are practically all in noncubic environments, it will give rise to a q_{MO} term. We have no estimate of the magnitude of this additional contribution.

Effect of Isomer-Shift Distribution

No account was taken of any possible isomer-shift distribution when fitting the EFG models to the EX and AB spectra; i.e., all quadrupole doublets were assumed to have the same δ. Both spectra are symmetric, which shows that either any distribution is negligible or, for almost every quadrupole doublet with a positive δ displacement from the δ mean, there is another doublet of equal intensity with a negative displacement, or both.

The isomer shift is a local effect, compared with the effect of EFG, as it depends essentially on the six Fe_0–O_1 interatomic distances. Displacement of an O_1 atom toward Fe_0 will lead to an increase in covalency and hence to an increase in the *s*-electron density at Fe_0 and a decrease in δ. This decrease will be proportional to the algebraic sum of the O_1 displacements toward Fe_0. In general the distribution of the δ shifts will be asymmetric, and the overall effect of both EFG and δ distributions will be to give an asymmetric Mössbauer spectrum. This is what would be expected for α-$LiFeO_2$ in the presence of short-range order. Since short-range order has been shown to exist in samples such as ours, the conclusion would be that the range of δ values in α-$LiFeO_2$ is not wide enough to be detected in our treatment of the experimental spectra.

Further Comments

To improve on model E would require self-consistent displacement of the oxygens *and* the cations from their idealized lattice sites. A suitable sample could in fact have been produced if the atoms in model D had been allowed to move so as to minimize the total energy, by introducing an attractive Fe–O potential in addition to the Fe–Fe repulsive potential. Considering the fairly narrow range of $|\overline{EFG}|$ values that was obtained in the various models by choosing reasonable values of the displacement and order parameters, this additional, by no means negligible, computational effort did not seem justified as long as the value of Q remains in doubt.

Conclusions

In spite of the various uncertainties and assumptions underlying the comparison of the calculated and the observed values of the quadrupole splitting in the ^{57}Fe Mössbauer spectrum of α-$LiFeO_2$, it appears that the observed splitting is largely accounted for by the distribution of q_{latt}, η_{latt} values arising from cationic disorder. Short-range order, such as has been shown (*7*) to exist in quenched samples, tends to increase the splitting somewhat, relative to the completely disordered crystal, when the oxygen atoms are displaced by less than about 0.2 Å from their idealized lattice sites. The observed splitting is thus not unduly large, even though it may seem so when one compares it with the splitting observed in the ordered γ-$LiFeO_2$ at 300°K, −0.26(6) mm/sec (*1*), and with the splittings reported for various simple, ordered Fe^{3+}_{HS} compounds. A reassessment of the validity of the models examined in this study will be possible when a more reliable estimate of the value of the nuclear quadrupole moment $Q(^{57}Fe)$ is available.

As could be expected, the major contribution to the value of $|\Delta_{obs}|$ comes from the nearest-neighbor cations M_1 (model A). However, a direct consequence of an approximation which includes only this limited environment is the overemphasis on the EFG = 0 contribution to the spectrum. Taking into account more distant cations (and oxygens) reduces the EFG = 0 contribution to a negligible fraction of the total. This overemphasis is even more serious in the EFG analysis of disordered perovskites (*13*), where the EFG = 0 contribution in a model including nearest-neighbor B cations only (cf. above) is 10/64 (≈15.6%), compared with 66/4096 (≈1.6%) for the NaCl-type solid solution, and hence inclusion of more distant ions in such cases is imperative.

It is of interest, for the analysis of nearest-neighbor cation models of equimolar binary cubic solid solutions, to note that the total

number $\Sigma N(k)$ of distinct $A_{m-k}B_k$ configurations engenders a relatively small number N' of distinct |EFG| values: the $N'/\Sigma N(k)$ ratio is, for a tetrahedron ($m = 4$), 3/5 (0.6); for an octahedron ($m = 6$), 4/10 (0.4); for a cube ($m = 8$), 8/22 ($\approx$0.364); and for a cuboctahedron ($m = 12$), 17/144 ($\approx$0.118). This progressive decrease in the ratio does not mean, however, that the geometric analysis can be easily extended to coordination figures with even larger numbers of vertices or to more distant cation environments (cf. under model B above).

Experimental

Cubic $LiFeO_2$ was prepared from reagent-purity Li_2CO_3 and a high-purity Fe powder enriched to contain 4% ^{57}Fe. The carbonate was dried, and the Fe powder was freshly reduced with H_2 immediately before use. The powders were dry-mixed, pressed, brought slowly to 900°C in a recrystallized-alumina crucible in air, and fired at that temperature; the total heating period was 24 hr. After grinding, a pellet pressed from the product was suspended on a thin Pt wire, fired in air at 900°C for 24 hr and quenched by being dropped from the vertical furnace into iced water. Two samples were prepared by this procedure on two different occasions. There was no noticeable difference between them.

The only lines present in the X-ray powder diffraction patterns of the product taken in a Guinier–Hägg camera (forward focusing, Cu$K\alpha$; internal Pt standard) were the sharp lines characteristic of the NaCl-type structure. The lattice parameter, $a_0 = 4.1556(5)$ Å ($\lambda(\mathrm{Cu}K\alpha_1) = 1.54056$ Å) was slightly smaller than that reported by Fayard (*14*) for a sample quenched from 750°C, 4.1575(3) Å.[7]

Mössbauer spectra were recorded to high statistics (typically 4–5 × 10^6 counts per channel) on standard constant-acceleration spectrometers at Exeter (EX, 200 channels) and Aberdeen (AB, 400 channels). The sources were ^{57}Co in Pd host lattices, and calibration was carried out with metallic Fe foils. Absorbers were prepared by dispersing the sample powder in acrylic disks. The AB absorbers did not contain more than 3 mg/cm^2 of total Fe and may thus be regarded as essentially thin. The total Fe content of the EX absorbers was about three times higher, which probably explains the greater linewidth (cf. Table VIII).

The spectrum of cubic $LiFeO_2$ at liquid-nitrogen temperature showed evidence of incipient magnetic ordering and at 4.2°K the six-line magnetic spectrum was fully resolved, in agreement with Ref. (*1*).

The use of the formulation $|\mathrm{EFG}| = (\frac{2}{3}\ \mathrm{tr}\ \mathbf{EFG}^2)^{1/2}$, $\mathrm{tr}\ \mathbf{EFG}^2 = (\Sigma V_{xx})^2 + (\Sigma V_{yy})^2 + (\Sigma V_{zz})^2 + 2[(\Sigma V_{xy})^2 + (\Sigma V_{xz})^2 + (\Sigma V_{yz})^2]$ saved on computing time in that the **EFG** matrix did not have to be inverted.

Because of the magnitude of the computing effort involved it was not feasible to sum over all the cations in sample B2a, i.e., for $r_{max} \to 12a \approx 50$ Å. A "limiting" |EFG| distribution was therefore simulated as follows.

The random numbers generator was called a number of times to produce B2a samples with different cation populations. For each of these it was determined how the |EFG| frequency in a given |EFG| interval varied with r_{max}, up to $r_{max} = 4a$. The |EFG| distributions of all these samples were then added, for each value of r_{max} examined, and smoothed by eye. A comparison of the smoothed distributions for successive values of r_{max} showed little change after $d_{0,6}$, and hence $d_{0,7}$ was chosen as the cutoff value. It is the smoothed curve for $r_{max} = d_{0,7}$ that is referred to as the "limiting" distribution B2a(∞).

[7] Fayard remarks that the a_0 of samples quenched from 950°C was several units in the fourth decimal smaller than that of samples quenched from 750°C. He attributes this to a decrease in the short-range order.

Acknowledgments

This investigation was supported by research grants from the National Research Council of Canada and from IBM Canada Ltd. to one of the authors (O.K.).

Appendix

Let $\mathbf{EFG}^\circ = r^5\mathbf{EFG}$ and $\Sigma r^5 V_{xx} = a_{11}$, etc. For Li_{12} and Fe_{12}, which have symmetry $m3m$, $a_{11} = \Sigma r^5 V_{xx} = \Sigma V^0_{xx} = 0$, etc. The quantities $r^5 V_{xx}$ and V^0_{xx}, etc., differ only by the charge factor u, i.e., $r^5\ V_{xx} = uV^0_{xx}$, etc. When the +1 charge at a vertex s is replaced by +3, a_{11}, a_{22}, etc., become, respectively, $2V^0_{xx}(s)$, $2V^0_{yy}(s)$, etc. Since V^0_{xx}, etc., are integers, a_{11}, etc., must also be integers. Moreover, every off-diagonal term $a_{ij} = 0$ (mod 6) (cf. Table II).

For det $\mathbf{EFG}^\circ$ = det (a_{ij}) to be zero, $(a_{11} + a_{22})(a_{12}^2 - a_{11}a_{22}) + 2a_{12}a_{13}a_{23} - a_{11}a_{23}^2 - a_{22}a_{13}^2 = 0$. Let $a_{12} = 6\alpha$, $a_{13} = 6\beta$, $a_{23} = 6\gamma$: $(a_{11} + a_{22})[a^2 - (a_{11}a_{22}/36)] = \beta^2 a_{22} + \gamma^2 a_{11} - 12\alpha\beta\gamma$. This equation in integers implies that $\alpha^2 - (a_{11}a_{22}/36)$ is an integer, i.e., $a_{11}a_{22} = 36\delta$. However, a_{11} and a_{22} are even, $a_{11} = 2\varepsilon$, $a_{22} = 2\zeta$, so that $\varepsilon\zeta = 3^2\delta$. Thus ε or ζ or both must contain 3 as a factor; hence $a_{11} = 0$ (mod 6) or $a_{22} = 0$ (mod 6) or both. But because of $V^0_{xx}(s) = 2$ or -4 and $|a_{11}| \leq 16$ (and similarly for $V^0_{yy}(s)$, etc.), $|a_{11}| = 0, 6, 12$ implies $|2\kappa - 4\lambda| = 0, 6, 12$, i.e., $k = \kappa + \lambda = 0$ (mod 3). Consequently the elements of $\mathbf{EFG}^\circ$ can only assume the values $0, \pm 6, \pm 12$.

References

1. D. E. Cox, G. Shirane, P. A. Flinn, S. L. Ruby, and W. J. Takei, *Phys. Rev.* **132**, 1547 (1963).
2. O. Knop, W. W. Barker, and P. S. White, *Acta Crystallogr. A* **31**, 461 (1975).
3. O. Knop, *Acta Crystallogr. A* **32**, 65 (1976).
4. O. Knop, E. M. Palmer, and R. W. Robinson, *Acta Crystallogr. A* **31**, 19, 704 (1975).
5. O. Knop, *Acta Crystallogr. A* **32**, 147 (1976).
6. R. D. Shannon, *Acta Crystallogr. A* **32**, 751 (1976).
7. M. Brunel and F. de Bergevin, *J. Phys. Chem. Solids* **30**, 2011 (1969).
8. F. de Bergevin and M. Brunel, *Bull. Soc. Fr. Min. Crist.* **91**, 621 (1968).
9. J. M. Cowley, *Acta Crystallogr. A* **29**, 537 (1973).
10. R. M. Sternheimer, *Phys. Rev.* **130**, 1423 (1963).
11. C. Ayasse, Ph.D. Thesis, Dalhousie University, Halifax, N.S., August 1972.
12. P. I. Kingsbury, *Acta Crystallogr. A* **24**, 578 (1968).
13. R. O. Bell, *J. Phys. Chem. Solids* **29**, 1 (1968).
14. M. Fayard, *Ann. Chim. (Paris)* **6**, 1279 (1961).